Published online 24 October 2017 *Nucleic Acids Research, 2017, Vol. 45, No. 22* ***13043–13055***
doi: 10.1093/nar/gkx970

Common TFIIH recruitment mechanism in global genome and transcription-coupled repair subpathways

Masahiko Okuda[1], Yuka Nakazawa[2,3], Chaowan Guo[3], Tomoo Ogi[3] and Yoshifumi Nishimura[1,*]

[1]Graduate School of Medical Life Science, Yokohama City University, 1-7-29 Suehiro-cho, Tsurumi-ku, Yokohama 230-0045, Japan, [2]Department of Genome Repair, Atomic Bomb Disease Institute, Nagasaki University, 1-12-4, Sakamoto, Nagasaki 852-8523, Japan and [3]Department of Genetics, Research Institute of Environmental Medicine (RIeM), Nagoya University, Furo-cho, Chikusa-ku, Nagoya 464-8601, Japan

Received July 05, 2017; Revised October 03, 2017; Editorial Decision October 07, 2017; Accepted October 10, 2017

ABSTRACT

Nucleotide excision repair is initiated by two different damage recognition subpathways, global genome repair (GGR) and transcription-coupled repair (TCR). In GGR, XPC detects DNA lesions and recruits TFIIH via interaction with the pleckstrin homology (PH) domain of TFIIH subunit p62. In TCR, an elongating form of RNA Polymerase II detects a lesion on the transcribed strand and recruits TFIIH by an unknown mechanism. Here, we found that the TCR initiation factor UVSSA forms a stable complex with the PH domain of p62 via a short acidic string in the central region of UVSSA, and determined the complex structure by NMR. The acidic string of UVSSA binds strongly to the basic groove of the PH domain by inserting Phe408 and Val411 into two pockets, highly resembling the interaction mechanism of XPC with p62. Mutational binding analysis validated the structure and identified residues crucial for binding. TCR activity was markedly diminished in *UVSSA*-deficient cells expressing UVSSA mutated at Phe408 or Val411. Thus, a common TFIIH recruitment mechanism is shared by UVSSA in TCR and XPC in GGR.

INTRODUCTION

Nucleotide excision repair (NER) is a ubiquitous and versatile DNA repair system that protects the genome from a wide range of risk factors such as ultraviolet (UV) radiation, chemical agents and metabolic byproducts that induce bulky DNA adducts. Defective NER gives rise to several inherited skin conditions (genodermatoses), such as xeroderma pigmentosum (XP), Cockayne syndrome (CS), trichothiodystrophy, and UV-sensitive syndrome (UV^{S}S) (1). NER is initiated by one of two damage recognition subpathways: global genome repair (GGR) (2,3) and transcription-coupled repair (TCR) (4,5). In GGR, the XP-related gene product XPC binds to RAD23B and CETN2, and then detects a DNA helix-distorting lesion on the entire genome (6,7) or, in some cases, UV light-damaged DNA-binding protein (UV-DDB) binds to a cyclobutane pyrimidine dimer (CPD) in a complementary manner (8,9). XPC then recruits the general transcription/repair factor TFIIH to the lesion (10,11), which verifies the presence and location of damage (12), and then opens up the damaged DNA for subsequent excision.

In TCR, by contrast, an elongating form of RNA polymerase II (RNA Pol IIo) first encounters the lesion on the transcribed DNA strand of actively transcribed genes (13). The stalled RNA Pol IIo molecule is then displaced (or backtracked) by the TCR-initiation complex, a multimolecular complex comprising CS complementation group proteins CSB (ERCC6) and CSA (ERCC8), UV-specific scaffold protein A (UVSSA) and ubiquitin-specific protease 7 (USP7); this provides space to enable TCR-specific factors to access the lesion for the DNA damage incision process (14). TFIIH is subsequently loaded onto the damaged site; in contrast to GGR, however, the mechanism responsible for recruitment of TFIIH in TCR remains elusive. After TFIIH recruitment, the two NER subpathways converge, and NER proceeds to perform excision and removal of a short oligonucleotide containing the lesion, followed by DNA resynthesis across the gap by polymerization and ligation using the opposite undamaged strand as a template.

UVSSA is a crucial TCR factor (15–17), and mutations in *UVSSA* cause UV^{s}S complementation group A (UV^{S}S-A), a rare autosomal recessive genodermatosis characterized by cutaneous photosensitivity without skin carcinoma and neurological abnormalities (18–21). UVSSA forms a complex with the deubiquitinating enzyme USP7 and, as men-

*To whom correspondence should be addressed. Tel: +81 45 508 7211; Fax: +81 45 508 7360; Email: nisimura@tsurumi.yokohama-cu.ac.jp

tioned above, cooperatively contributes to the processing of RNA Pol IIo stalled at damage sites, in addition to stabilization of CSB by protecting against UV-induced degradation through regulation of ubiquitination and deubiquitination (15–17,22,23).

TFIIH is a 10-subunit protein complex that functions in transcription and cell cycle, as well as NER (24). Its p62 subunit has a pleckstrin homology (PH) domain at its N terminus (residues 1–108 in human; hereafter termed p62 PH), which has proven to be crucial as a hub responsible for recruiting the TFIIH complex to the sites necessary for its function. In GGR, for example, XPC recruits TFIIH mainly via interaction with p62 PH (25,26). In transcription, the general transcription factor TFIIEα (27,28) and transcriptional activators such as the tumor suppressor p53 (29,30), erythroid Kruppel-like factor (31), cell cycle controlling factor DP1 (32), and a member of the NF-κB family p65 (33) all target p62 PH; furthermore, viral transcriptional activators, herpes simplex virus protein VP16 (34,35) and Epstein–Barr virus nuclear antigen 2 (36) also target this domain of TFIIH.

Regarding the interactions of mammalian p62 PH and its binding partners, four structures of human p62 PH in complex with XPC, TFIIEα, p53 and DP1 have been determined (26,28,30,32) and reveal a common structural principle for the recognition of p62 PH: (i) an intrinsically disordered acidic region of the p62 PH-binding protein forms an extended string-like conformation in a binding-coupled manner; (ii) the acidic region in the p62 PH-binding protein interacts with an exposed basic surface of p62 PH via extensive electrostatic contacts; (iii) the insertion of a phenylalanine or a tryptophan residue surrounded by several acidic residues into a pocket in p62 PH is necessary and essential for specific binding.

In this study, we focused on the process of TFIIH recruitment in TCR. We identified a short acidic region in UVSSA that is similar to the p62 PH-binding region of XPC and also meets the structural principles of p62 PH recognition, and then tested whether this region is responsible for the recruiting of TFIIH in TCR. Binding analyses using isothermal titration calorimetry (ITC) and nuclear magnetic resonance (NMR) spectroscopy demonstrated that a stable complex is formed between the UVSSA acidic region and p62 PH. Using NMR spectroscopy, we determined structure of the UVSSA–p62 PH complex, which showed significant resemblance to the XPC–p62 PH complex. Mutational binding analysis by ITC further clarified the role of key residues suggested by the tertiary structure. Finally, mutant UVSSA proteins with amino acid substitutions of residues identified as critical for p62 binding elicited a significant reduction in transcription-coupled NER activity, suggesting that the UVSSA–TFIIH p62 interaction is crucial for progression of the TCR initiation process to unwind DNA damage.

MATERIALS AND METHODS

Protein expression and purification

Unlabeled or $^{13}C/^{15}N$-labeled human TFIIH p62 PH (residues 1–108) and unlabeled or $^{13}C/^{15}N$-labeled human UVSSA (residues 390–434) were prepared as previously described (28). In brief, p62 or UVSSA was expressed as fusion product with glutathione S-transferase (GST) in a pGEX-4T vector (GE Healthcare) in *Escherichia coli* BL21(DE3) cells (Merck Millipore). The lysed supernatant was loaded onto a glutathione Sepharose column (GE Healthcare), and the eluate was digested with thrombin to remove the GST tag. After concentration with an Amicon Ultra device (Merck Millipore), the sample was purified on a Superdex75 column (GE Healthcare).

Peptide preparation

Unlabeled wild-type and mutated peptides of human UVSSA (residues 399−419) were purchased from Sigma Genosys and GenScript.

ITC

The K_d values of the interaction between p62 PH and UVSSA (residues 390−434 and residues 399−419) were measured by ITC using a VP-ITC calorimeter (MicroCal). Calorimetric titrations between 250 μM UVSSA in the syringe (25 × 20 μl injections) and 2 ml of 25 μM p62 PH in the cell were carried out in 20 mM potassium phosphate (pH 6.8) at 20°C. Each injection took 4 s, with a preinjection delay of 210 s and a syringe stirring speed of 307 rpm. Data were analyzed by using the Origin software package (MicroCal).

NMR chemical shift perturbation

Unlabeled p62 PH was added to 0.4 mM $^{13}C/^{15}N$-labeled UVSSA at a molar ratio of 1.0:1.2 in 20 mM potassium phosphate (pH 6.8), 5 mM deuterated DTT, and 10% D_2O. Unlabeled UVSSA was added to 0.4 mM $^{13}C/^{15}N$ -labeled p62 PH at a molar ratio of 1.0:1.2 in the same buffer. $^{1}H,^{15}N$ HSQC spectra were acquired before and after the addition of unlabeled samples at 32°C on Bruker AVANCE III HD 950MHz spectrometers equipped with a triple-resonance TCI cryogenic probe. Backbone resonances were assigned by using a combination of CBCA(CO)NH, CBCANH, HNCO and HN(CA)CO signals. Spectra were processed by NMRPipe (37) and analyzed by NMRView (38).

NMR spectroscopy

$^{13}C/^{15}N$-labeled UVSSA (residues 390–434) was mixed with unlabeled p62 PH at a molar ratio of 1.0:1.2 in 20 mM potassium phosphate (pH 6.8), 5 mM deuterated DTT, and either 10% D_2O or 99.9% D_2O to prepare the complex at 0.4 mM. In the same way, $^{13}C/^{15}N$-labeled p62 PH was mixed with unlabeled UVSSA. NMR experiments were performed at 32°C on Bruker AVANCE III HD 600 MHz and 950 MHz spectrometers, each equipped with a cryogenic probe. Backbone and side-chain resonances were assigned by using standard triple-resonance NMR experiments (39). Stereospecific assignments were obtained from a combination of HNHB, HN(CO)HB, HNCG, HN(CO)CG and ^{13}C-edited and ^{15}N-edited NOESY-HSQC (τ_m = 50 ms) spectra. Intramolecular distance restraints were obtained

from ^{15}N-edited NOESY-HSQC (τ_m = 50 and 150 ms) and ^{13}C-edited NOESY-HSQC (τ_m = 50 and 100 ms) spectra. Intermolecular distance restraints were obtained from ^{13}C, ^{15}N filtered/edited NOESY (τ_m = 120 and 150 ms) spectra. Side-chain torsion angles, $\chi 1$ and $\chi 2$, were obtained from a combination of HNHB, HN(CO)HB, HNCG, HN(CO)CG and ^{13}C-edited and ^{15}N-edited NOESY-HSQC (τ_m = 50 ms) spectra. Hydrogen bond restraints were obtained by backbone amide H/D-exchange experiments. Spectra were processed by NMRPipe (37) and analyzed by NMRView (38).

Structure calculation

In total, 197 and 2498 NOE-derived distance restraints were collected for UVSSA and p62 PH, respectively (Table 1). In addition, 96 hydrogen bond restraints were collected for p62 PH, and 17 and 267 dihedral angle restraints were collected for UVSSA and p62 PH, respectively. For the intermolecular distance restraints, 359 intermolecular NOEs and 2 hydrogen bond restraints were collected. Interproton distance restraints derived from NOE intensities were grouped into four distance ranges, 1.8−2.7 Å (1.8−2.9 Å for NOEs involving HN protons), 1.8−3.3 Å (1.8−3.5 Å for NOEs involving HN protons), 1.8−5.0 and 1.8−6.0 Å, corresponding to strong, medium, weak and very weak NOEs, respectively. The upper limit was corrected for constraints involving methyl groups, aromatic ring protons, and non-stereospecifically assigned methylene protons. Dihedral angle restraints for φ and ψ were obtained from analysis of the backbone chemical shifts with TALOS+ (40). $\chi 1$ and $\chi 2$ angles were restrained $\pm 30^\circ$ for three side-chain rotamers. Structure calculations were performed by distance geometry and simulated annealing using the program Xplor-NIH (41,42). In total, 100 structures were calculated. All structures were then subjected to water refinement (43), in which the structures were immersed in a 7.0 Å layer of water molecules. After minimization with 120 steps, a heating stage from 100 to 500 K with 200 steps of molecular dynamics for every 100 K increment, a refinement stage with 2500 steps at 500 K, and a cooling stage from 500 to 25 K with 200 steps for every 25 K decrement were carried out. The refinement protocol was finished with 200 steps of minimization. Structural statistics for the 20 best structures are summarized in Table 1. Structures were analyzed and displayed by using PROCHECK-NMR (44), CHIMERA (45,46), and PyMol (http://www.pymol.org).

Recovery of RNA synthesis (RRS) assay

The RRS assay has been described previously (15,47,48). TCR-deficient (Kps3) and TCR-proficient (48BR) control primary fibroblasts were plated in 96-well plates. For virus complementation experiments, cells were infected with lentiviruses expressing V5-tagged wild-type, or various mutant UVSSA cDNAs for 48 h prior to UV irradiation. Cells were UV-irradiated (12 J/m^2 of 254 nm UV-C) and incubated for 12 h for RNA synthesis recovery. RRS was measured by the fluorescence-based ethynyluridine (EU) incorporation assay. In brief, cells were incubated for 2 h after RNA synthesis recovery in medium containing 100 μM 5-ethynyluridine (EU), followed by Click reaction to conjugate Alexa488 fluorescent dye to incorporated EU. Cells were stained with 20 ng/ml of DAPI and Alexa647-conjugated anti-V5 antibody to select infection-positive cells for the RRS measurement. Fluorescent image acquisition and data processing were automated by using the ArraySCAN^{VTI} system (Thermo Scientific). The RRS in V5-positive cells was calculated.

Immunoprecipitation

Either V5-tagged wild type or various mutant UVSSA proteins were ectopically expressed in HEK293FT cells. Immunoprecipitation of the UVSSA proteins was performed on the cell extracts using anti-V5 agarose beads (MBL). Immunoprecipitated protein samples were separated on 5–20% gradient SDS-PAGE gels, blotted onto PVDF membranes (PALL), and analyzed by western blotting with antibodies specific for V5-tag and p62.

RESULTS

Identification of a potential TFIIH p62 PH-binding region in UVSSA

Despite being a crucial and fundamental process, the mechanism of TFIIH recruitment in TCR has remained elusive. To obtain clues on this process, we first examined the amino acid sequences of the TCR-specific proteins CSA, CSB, UVSSA, USP7, XAB2, HMGN1 and TFIIS. Intriguingly, we found that only UVSSA possesses a sequence similar to the p62 PH-binding regions of XPC and TFIIEα, located at residues 400–413 of human UVSSA (Figure 1A). In this region, eight consecutive acidic amino acids (Glu400–Asp407) are followed by an aromatic residue (Phe408), and the third residue from the aromatic residue is a valine (Val411). In previous studies, we observed that a key aromatic residue, either phenylalanine or tryptophan, in the acidic regions of XPC, TFIIEα, p53 and DP1 is inserted into a pocket (hereafter termed 'pocket 1') of p62 PH. In addition, the third valine residue from the aromatic residue in XPC and TFIIEα inserts its side-chain into another pocket (hereafter termed 'pocket 2'), leading to the higher p62 PH binding affinities of the acidic regions of XPC and TFIIEα as compared with p53 and DP1 (26,28,49). Furthermore, the third residue is a glutamate in p53 and an asparagine in DP1, and the substitution of asparagine with valine in DP1 leads to increased binding affinity (32). As a result, we presumed that the acidic region of UVSSA may bind strongly to p62 PH for recruitment of TFIIH.

As shown in Figure 1B, UVSSA contains two conserved domains: the VHS (Vps-27, Hrs, and STAM) domain, and DUF2043 (domain of unknown function) domain. The presumed binding region to p62 PH is located in the central region between these domains. Although the number of consecutive acidic amino acids varies across species, the presumed binding sequence is well conserved (Figure 1A). To our knowledge, however, no particular functions have as yet been identified for this acidic region. The presumed binding region is likely to be an intrinsically disordered region (IDR) similar to the acidic regions of XPC and other p62 PH-binding partners (Figure 1B).

Table 1. Structural statistics for the 20 best structures of the complex formed between $UVSSA_{390–434}$ and TFIIH p62 PH

	UVSSA		TFIIH p62
Experimental restraints			
Total NOE	197		2498
Intraresidue	19		375
Sequential (i - j = 1)	131		616
Medium-range (1 < i – j < 5)	47		414
Intramolecular long-range (i – j ≥ 5)	0		1093
Intermolecular		359	
Hydrogen bond	0		48 × 2
Intermolecular		1 × 2	
Number of dihedral restraints			
φ	7		98
ψ	7		97
χ1	3		62
χ2	0		10
Statistics for structure calculations			
R.m.s. deviations from experimental restraints[a]			
Distance (Å)		0.032 ± 0.001	
Dihedral (°)		0.285 ± 0.028	
R.m.s. deviations from idealized covalent geometry			
Bonds (Å)		0.00483 ± 0.00008	
Angles (°)		0.645 ± 0.015	
Improper (°)		0.660 ± 0.025	
Coordinate precision			
Average pairwise r.m.s. deviation from the mean structure			
Backbone atoms (Å)	0.51 ± 0.16[b]	0.50 ± 0.11[c]	0.46 ± 0.10[d]
Heavy atoms (Å)	1.24 ± 0.25[b]	1.16 ± 0.16[c]	1.12 ± 0.16[d]
Ramachandran plot statistics			
Residues in most favored regions (%)		85.8[e]	
Residues in additional allowed regions (%)		12.9[e]	
Residues in generously allowed regions (%)		0.2[e]	
Residues in disallowed regions (%)		1.1[e]	

[a]None of the structures exhibited distance violations >0.5 Å, dihedral angle violations >5°.
[b]The value was calculated over residues 402–417 of the UVSSA in the complex.
[c]The value was calculated over residues 402–417 of the UVSSA and residues 7–104 of the TFIIH p62 PH domain in the complex.
[d]The value was calculated over residues 7–104 of the TFIIH p62 PH domain in the complex.
[e]The value was calculated over residues 402–417 of the UVSSA and residues 7–104 of the TFIIH p62 PH domain in the complex.

UVSSA binds with high affinity to p62 PH of TFIIH

To examine whether the presumed binding region of UVSSA has affinity for p62 PH, and if so, its strength, we analyzed the interaction by using ITC. We prepared a fragment of human UVSSA corresponding to residues 390–434 ($UVSSA_{390–434}$), which contains the presumed binding region (residues 400–413) and used it as a titrant. The ITC data indicated that the fragment strongly and specifically binds to p62 PH in an exothermic reaction (ΔG = –9.6 kcal·mol^{-1}; $T\Delta S$ = 4.0 kcal·mol^{-1}; ΔH = –5.6 kcal·mol^{-1}; binding stoichiometry = 1:1; K_d = 71.4 ± 16.7 nM) (Figure 2A). The binding affinity was equivalent to that of XPC (K_d = 60–140 nM) and TFIIEα (K_d = 95 nM), and higher than that of p53 (K_d = 960 nM) and DP1 (K_d = 980 nM) (26,50).

We then investigated which residues in the binding fragment of UVSSA are affected on binding to p62 PH by using NMR spectroscopy. In the free form, all backbone amide resonances of $UVSSA_{390–434}$ were observed within a narrow range between 7.8 and 8.6 ppm on the ^{1}H axis in the ^{1}H–^{15}N HSQC spectrum, indicating that the fragment is an IDR (Figure 2B upper panel and Supplementary Figure S1, black signals). By contrast, the addition of unlabeled p62 PH significantly changed the position (chemical shift) of several backbone amide resonances of $UVSSA_{390–434}$ (Figure 2B upper panel and Supplementary Figure S1, blue signals). These resonances corresponded to residues from Asp405 to Glu415, suggesting that the presumed binding acidic region indeed interacts with p62 PH. In the complementary experiment, i.e. the addition of unlabeled $UVSSA_{390–434}$ to ^{15}N-labeled p62 PH, the resonances of several residues of p62 PH (Lys19, Glu53 to Val68, Thr74 to Phe79, and Asp94) displayed relatively large chemical shift changes when $UVSSA_{390–434}$ was added (Figure 2B lower panel and Supplementary Figure S2). Similar chemical shift changes in these residues have been previously observed when XPC and other p62 PH-binding partners are added to TFIIH p62 PH. Collectively, these results indicate that $UVSSA_{390–434}$ is disordered in the unbound state but, on encountering p62 PH, its acidic region adopts a certain structure and binds to the surface of p62 PH at a region similar to that bound by the XPC, TFIIEα, p53 and DP1 acidic region.

Binding to TFIIH p62 PH induces an extended string-like structure in the IDR of UVSSA

The binding analyses by ITC and NMR spectroscopy clearly indicated that $UVSSA_{390–434}$ and p62 PH form a stable complex in solution. Next, to elucidate the recognition mechanism, we solved the structure of the complex by using 950 MHz NMR spectroscopy. In total, 197 nuclear Over-

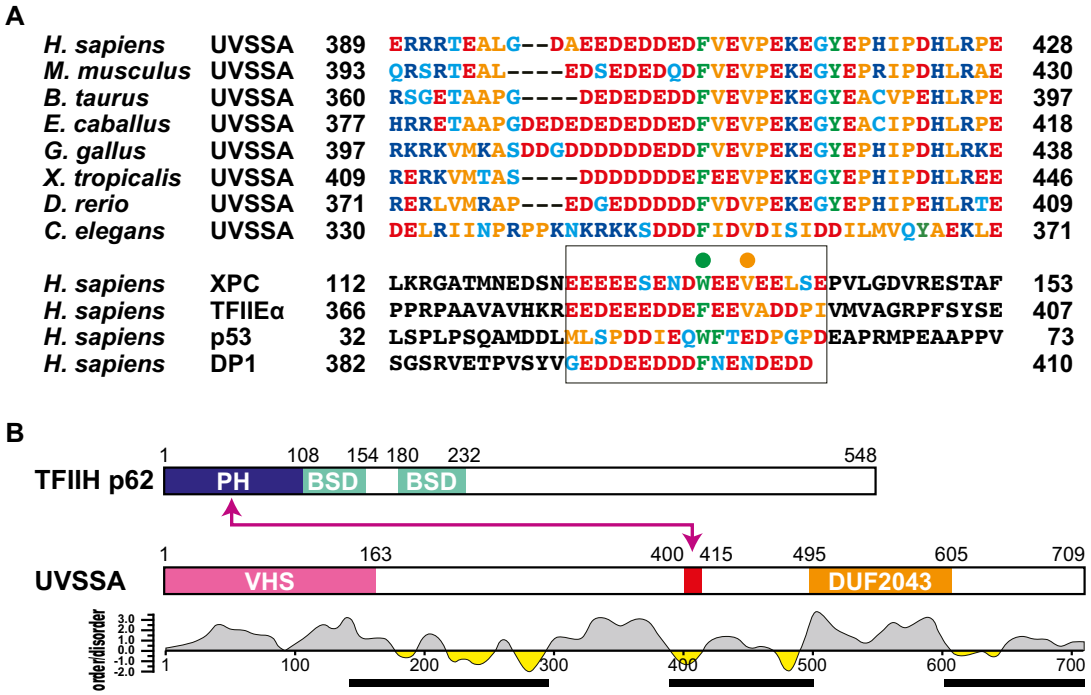

Figure 1. Amino acid sequence and domain organization of UVSSA. (**A**) Alignment of the amino acid sequences of UVSSA and the TFIIH p62 PH-binding regions of human XPC, TFIIEα, p53, and DP1. Green and orange circles above the sequence of XPC indicate the amino acids that insert into pocket 1 and pocket 2 in p62 PH, respectively. (**B**) Domain organization of TFIIH p62 and UVSSA. Intrinsically disordered regions in UVSSA predicted by IDEAL (55) are indicated by the black bars.

hauser effect (NOE)-derived distance restraints and 17 dihedral angle restraints collected for UVSSA, and 2498 NOE-derived distance restraints, 96 hydrogen bond restraints, and 267 dihedral angle restraints collected for p62 PH were used to define each structure in the complex. For UVSSA, these restraints alone were not enough to define the structure owing to its elongated conformation; however, 359 intermolecular NOE-derived distance restraints and 2 intermolecular hydrogen bond restraints fully determined its structure, as well as the structure of the whole complex (Figure 3A and Table 1).

In terms of the coordinate precision of UVSSA, p62 PH, and the whole complex, the r.m.s.d. was, respectively, 0.51 ± 0.16, 0.46 ± 0.10 and 0.50 ± 0.11 Å for the backbone atoms; and 1.24 ± 0.25, 1.12 ± 0.16 and 1.16 ± 0.16 Å for the heavy atoms (Table 1). As shown in Figure 3A, the structure of p62 PH bound to UVSSA is essentially the same as its structure in the unbound state (51) and those bound to XPC and other p62 PH binding proteins. By contrast, UVSSA, which is disordered in the free state, forms an extend string-like structure upon binding to p62 PH, and widely wraps its acidic string around the basic surface of p62 PH, which is formed by a loop between the β1 and β2 strands in the first antiparallel β sheet (β1–β4), the second antiparallel β sheet (β5–β7), and the C-terminal part of the α1 helix of p62 PH (Figure 3B–E). Residues 402–417 of UVSSA are well ordered, whereby residues 409–412 form the β0 strand, which makes an anti-parallel β sheet with the β5 strand of p62 PH.

UVSSA and the GGR factor XPC use a similar mode of TFIIH p62 PH recognition

The determined structure revealed that the TCR-specific factor UVSSA and the GGR-specific factor XPC bind to almost the same positively charged molecular surface of p62 PH (Figure 4). Therefore, to examine further the p62 PH recognition mode of UVSSA, we compared it with that of XPC and clarified the similarities and differences of TFIIH recognition between TCR and in GGR.

UVSSA possesses eight consecutive acidic amino acids located at residues 400–407 in the N terminus of the binding region (Figure 5A). This highly acidic polypeptide chain forms an extended conformation and runs along a positively charged path on the surface of p62 PH, making electrostatic interactions with Lys18 and Lys19 in the loop between strands β1 and β2 and Lys60 and Lys62 in the loop between strands β5 and β6 of p62 PH. Very similar extensive electrostatic interactions are observed in the XPC–p62 PH complex, where XPC makes contacts via seven acidic residues including five consecutive glutamate amino acids located at residues 124–132 (Figure 5B). These acidic amino acids of XPC electrostatically interact with the same lysine residues of p62, namely, Lys18, Lys19, Lys60 and Lys62.

As mentioned above, p62 PH has two hydrophobic pockets, 'pocket 1' and 'pocket 2' on the binding surface (Figure 4B). Pocket 1 is occupied by the aromatic ring of UVSSA Phe408, which is located immediately after the stretch of acidic amino acids (Figure 5C). In the pocket, Phe408 makes van der Waals contacts with the aliphatic parts of Lys54 and Ser56, in addition to amino (δ_+)–aromatic (π)

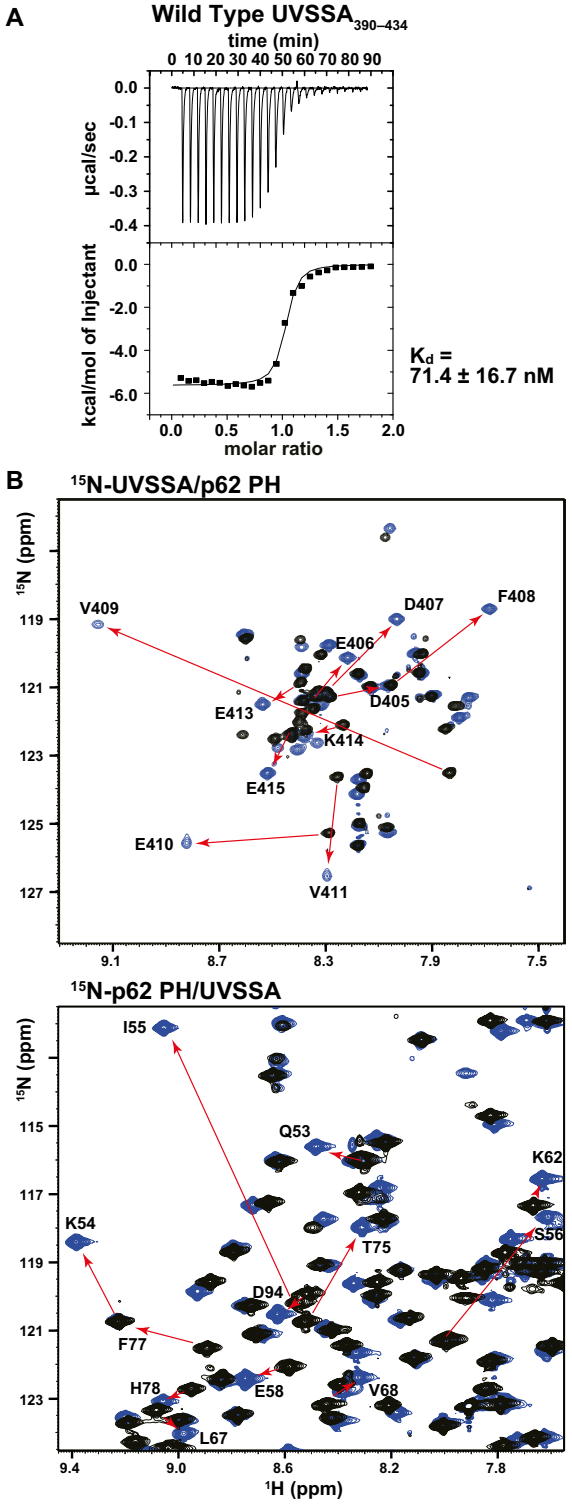

Figure 2. Specific binding of UVSSA to TFIIH p62 PH. (**A**) Isothermal titration calorimetry for the binding of $UVSSA_{390–434}$ to TFIIH p62 PH. Shown are thermogram (upper panel) and binding isotherm (lower panel) of the calorimetric titration. Titrant: wild-type $UVSSA_{390–434}$. (**B**) NMR chemical shift perturbation for ^{15}N-labeled $UVSSA_{390–434}$ with TFIIH p62 PH (upper panel) and for ^{15}N-labeled TFIIH p62 PH with $UVSSA_{390–434}$ (lower panel). Shown in overlay of ^{1}H–^{15}N HSQC spectra before (black) and after (blue) the addition of unlabeled sample. Selected regions are shown here (see full region in Supplementary Figures S1 and S2). Residues showing a large chemical shift change are labeled.

interactions (52) with Gln64, Gln66, and Asn76 in the second antiparallel β sheet of p62 PH. Correspondingly, in the XPC–p62 PH complex, the indole ring of XPC Trp133 inserts into pocket 1 in the same direction as the aromatic ring of UVSSA Phe408, and interacts with the same residues of p62 (Figure 5D).

Meanwhile, pocket 2 of p62 PH is packed with Val411 in the β0 strand of UVSSA (Figure 5E). Val411 inserts its two methyl groups into the pocket in a specific orientation and makes hydrophobic contacts with Ile55 and the aliphatic parts of Gln53 and Lys93 of p62. Glu410 makes electrostatic and van der Waals contacts with Lys54 in strand β5 of p62 (Figure 5E). XPC has the same amino acids, Val136 and Glu135, at the corresponding positions in the XPC–p62 PH complex, and these two residues make identical interactions with the p62 residues (Figure 5F). In the UVSSA–p62 PH complex, Val409 of UVSSA makes hydrophobic contacts with Ile55 and Pro57 of p62 (Figure 5E). Glu134, the corresponding residue of XPC, also makes contacts with Ile55 and Pro57 of p62, but this acidic residue seems to compensate for the weaker hydrophobic interaction by making electrostatic contact with Arg89 of p62 (Figure 5F).

The sequence after Val411 of UVSSA is considerably different from the corresponding sequence of XPC except for a glutamate residue (Glu413 in UVSSA; Glu138 in XPC), which makes van der Waals contacts with Pro101 and electrostatic contacts with Lys104 in the α1 helix of p62 (Figure 5G and H). Nevertheless, both polypeptide chains pass by the C terminus of the α1 helix, interacting with almost identical residues in this helix (Figure 5G and H). Similar to Leu139 of XPC, Lys414 of UVSSA makes hydrophobic contacts with the aliphatic portions of Gln97 and Gln98 of p62. Tyr417 of UVSSA also makes contacts with Gln98 of p62, and at the same time, with Lys414 via cation-π interaction. Similar to Ser140 of XPC, Glu415 of UVSSA makes contacts with Pro101 of p62. Regarding UVSSA, an electrostatic interaction between Glu418 and Lys102 of p62 was suggested in some structures of the NMR ensemble by the water-refined structure calculation. A similar suggestion was previously made for Glu141 of XPC. Thus, UVSSA specifically recognizes p62 PH through an interaction mode that is nearly identical to that of XPC.

Aromatic and hydrophobic residues of UVSSA are required for strong binding

In both the UVSSA–p62 PH and XPC–p62 PH complex structures, a single aromatic amino acid (Phe408 in UVSSA; Trp133 in XPC) and a single valine (Val411 in UVSSA; Val136 in XPC), respectively, insert into pocket 1 and 2 in p62 PH. Our previous study showed that alanine substitution of each of these residues in XPC, especially that of Trp133, markedly reduces the binding activity (26). Next, therefore, we examined whether this type of site-specific mutation would reduce the binding affinity of UVSSA by using ITC. First, we compared the binding activity of $UVSSA_{390–434}$, which was prepared from an expression system in *E. coli* and used for structure determination, and that of a smaller chemically synthesized peptide of $UVSSA_{399–419}$, which encompasses only the binding site. The two fragments of UVSSA showed almost the

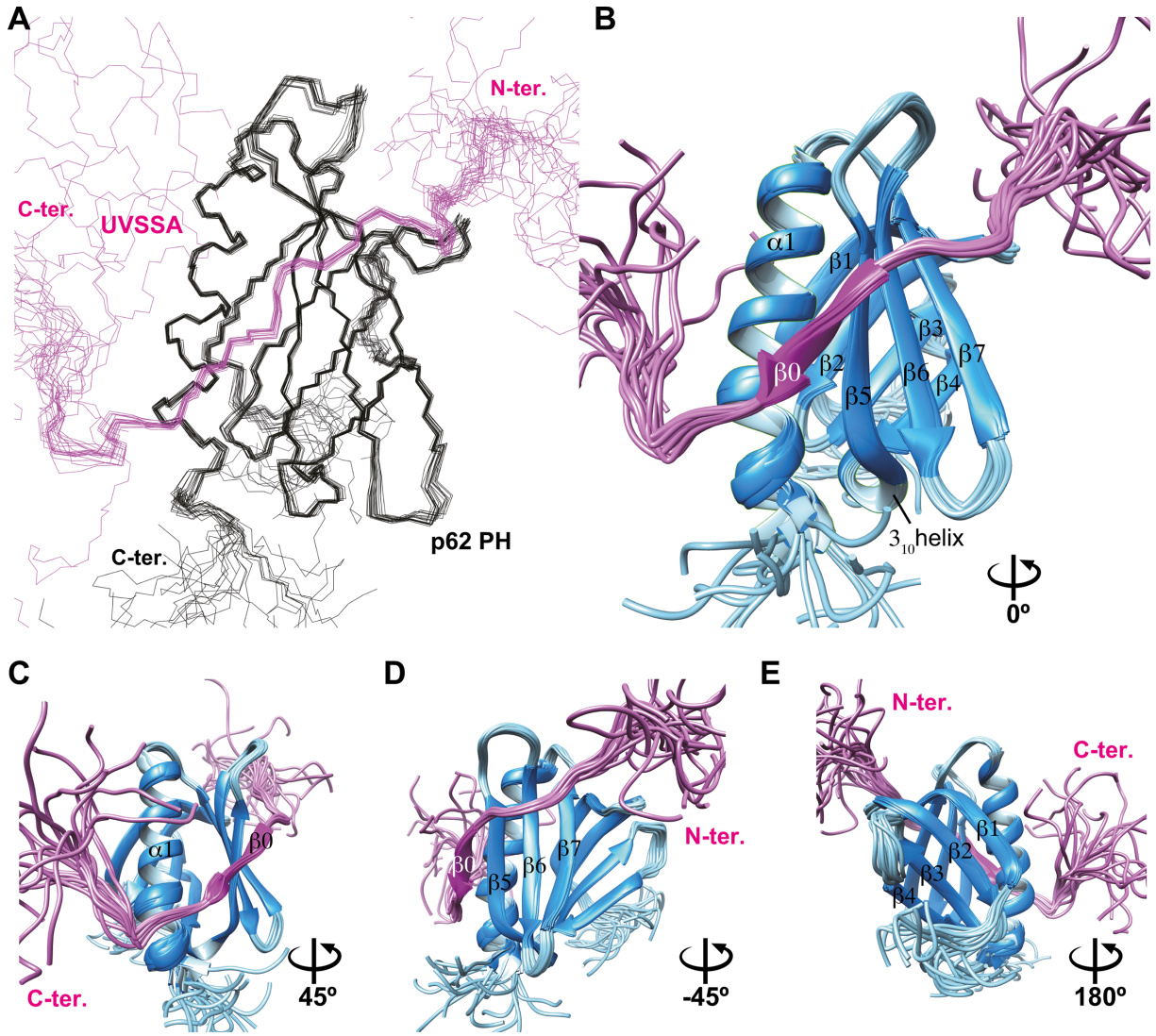

Figure 3. Structure of the complex between UVSSA and TFIIH p62 PH. (**A**) The 20 best solution structures represented as a line diagram. UVSSA and p62 are shown in magenta and black, respectively. (**B**–**E**) The 20 best solution structures represented as a ribbon diagram. UVSSA and p62 are shown in magenta and blue, respectively. For clarity, the four N-terminal residues and the nine C-terminal residues of UVSSA$_{390–434}$ have been omitted. The structures in C, D, and E are rotated by 45, -45, and 180 degrees, respectively, relative to the structures in A and B.

same binding activity (both K_ds ≅ 70 nM) (Figures 2A and 6A); therefore, we used UVSSA$_{399–419}$ peptides for the mutational analysis.

Substitution of Phe408 (F408A) of UVSSA with alanine led to a marked loss of binding activity (Figure 6B). The K_d was 5.1 ± 0.6 μM, which is two orders of magnitude larger than that of the wild-type peptide. Although not such a marked decrease, the V411A peptide also showed reduced binding activity with a K_d (380.2 ± 82.3 nM) 5-fold greater than that of wild type (Figure 6C). Hence, we confirmed that these two pocket-packing residues of UVSSA are as significant for strong binding to TFIIH as the corresponding residues of XPC.

We also tested the significance of Val409 of UVSSA, which makes hydrophobic contacts with Ile55 and Pro57 of p62 PH (Figure 5E). The V409A peptide showed a 3-fold reduction in binding affinity (K_d = 217.9 ± 40.2 nM) (Figure 6D). Thus, Val409 is important for strong binding to TFIIH, but its contribution is a little less than that of Val411.

Binding deficient UVSSA mutants fail to restore normal RNA synthesis recovery

To verify the cellular significance of the interaction of UVSSA and p62, we examined TCR activity in cells by measuring the recovery of RNA synthesis after UV irradiation. We generated Kps3 cells lines (originating from a *UVSSA* deficient UV^{S}S patient) expressing UVSSA mutants in which each amino acid responsible for the interaction with p62 PH was substituted with alanine or another residue, as shown in Figure 7. Substitution of Phe408 or Val411 in UVSSA with alanine caused a significant reduction of TCR activity. The mutant in which Phe408 was substituted with alanine showed a large reduction; on the other

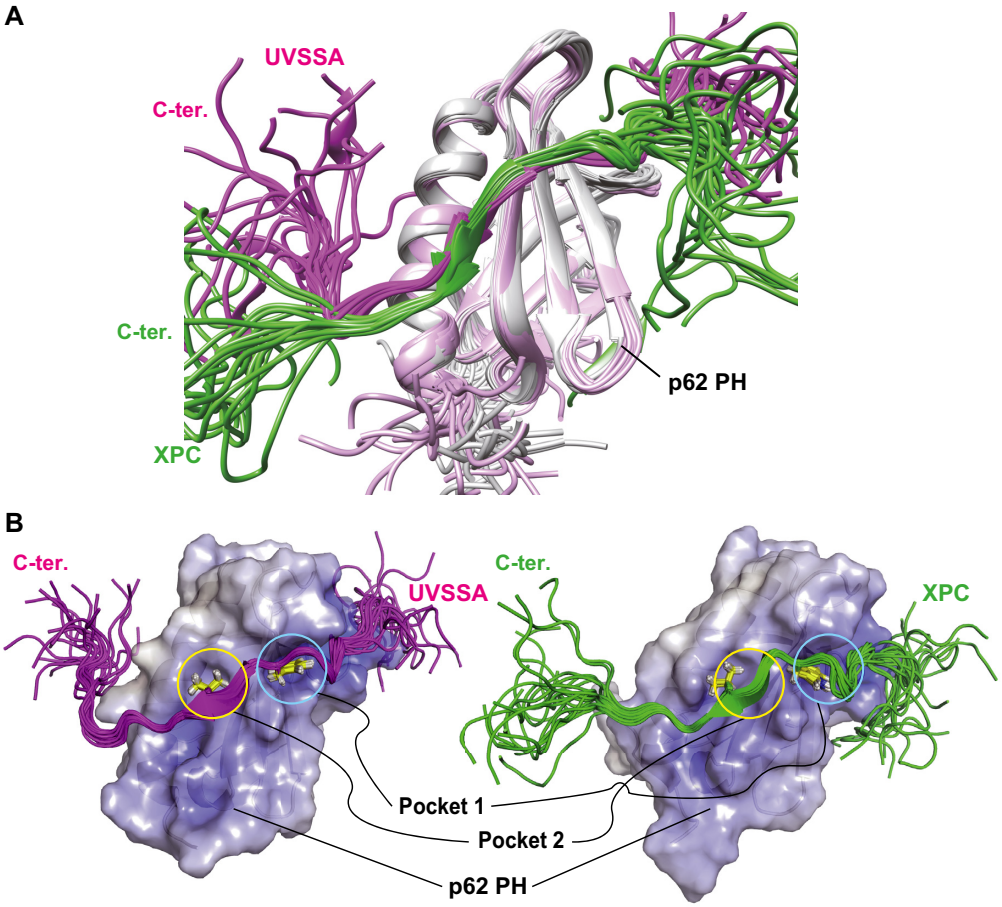

Figure 4. Structural comparison of the UVSSA–p62 PH and XPC–p62 PH complexes. (**A**) Superimposition of the best 20 structures of the UVSSA–p62 PH complex (magenta/pink) and those of the XPC–p62 PH complex (green/grey). (**B**) Binding surface of p62 PH in complex with UVSSA (left) and XPC (right). The electrostatic potential surfaces are shown. Positive potential is shown in blue, and negative potential in red. UVSSA and XPC are shown in stick representation (best 20 structures).

hand, the mutant substituted with tryptophan to resemble XPC did not exhibit such a marked reduction. In the case of Val411, substitution with glutamic acid or asparagine to resemble p53 or DP1 led to diminished TCR activity, similar to the effect of alanine substitution. The replacement of Val409 with alanine also led to a reduction of TCR activity somewhat, but the reduction was not as marked as compared with substitution of Phe408 or Val411. These findings are well correlated with the *in vitro* binding activities measured for the mutants (Figure 6). Substitution of each of the acidic residues, Glu401, Glu410 and Glu413, with alanine, lysine or arginine did not strongly alter the TCR activity of each mutant. Thus, the three acidic residues of UVSSA are not likely to play an essential role in the interaction with p62 PH; rather, the net charge of the acidic string of UVSSA seems to be important for p62 PH binding. Regardless, these findings indicate that the interaction between UVSSA and p62 PH is essential for TCR.

Next, we examined the interaction of full-length UVSSA with p62 by immunoprecipitation (Figure 7B). A variant in which the key residue Phe408 of UVSSA was replaced with tryptophan retained strong binding affinity to p62. On the other hand, UVSSA mutants with deletion of residues 390–434, replacement of Phe408 with alanine, and replacement of Val411 with asparagine showed significantly decreased binding affinity, although they still bound to p62. Their weaker binding affinities remain to be elucidated.

DISCUSSION

In TCR, the important molecular mechanism underlying the recruitment of TFIIH to a site of DNA damage has so far remained elusive. TFIIH is known to interact with multiple TCR factors; however, the protein that is responsible for recruiting TFIIH in TCR has not been identified. Elucidating the interplay among the TCR factors involved in each step is essential for a comprehensive understanding of NER. For this purpose, here we focused on identification of the factor that recruits TFIIH in TCR. The TFIIH complex is required not only for NER but also for transcription. Intriguingly, p62, a subunit of TFIIH, is often involved when TFIIH is recruited to damaged sites in the genome and transcription initiation sites. Notably, the proteins so far identified as involved in TFIIH recruitment, such as XPC in the GGR pathway, and TFIIEα, p53, and DP1 in transcription initiation, bind to an almost identical basic surface in the N-terminal PH domain of p62 via an intrinsically dis-

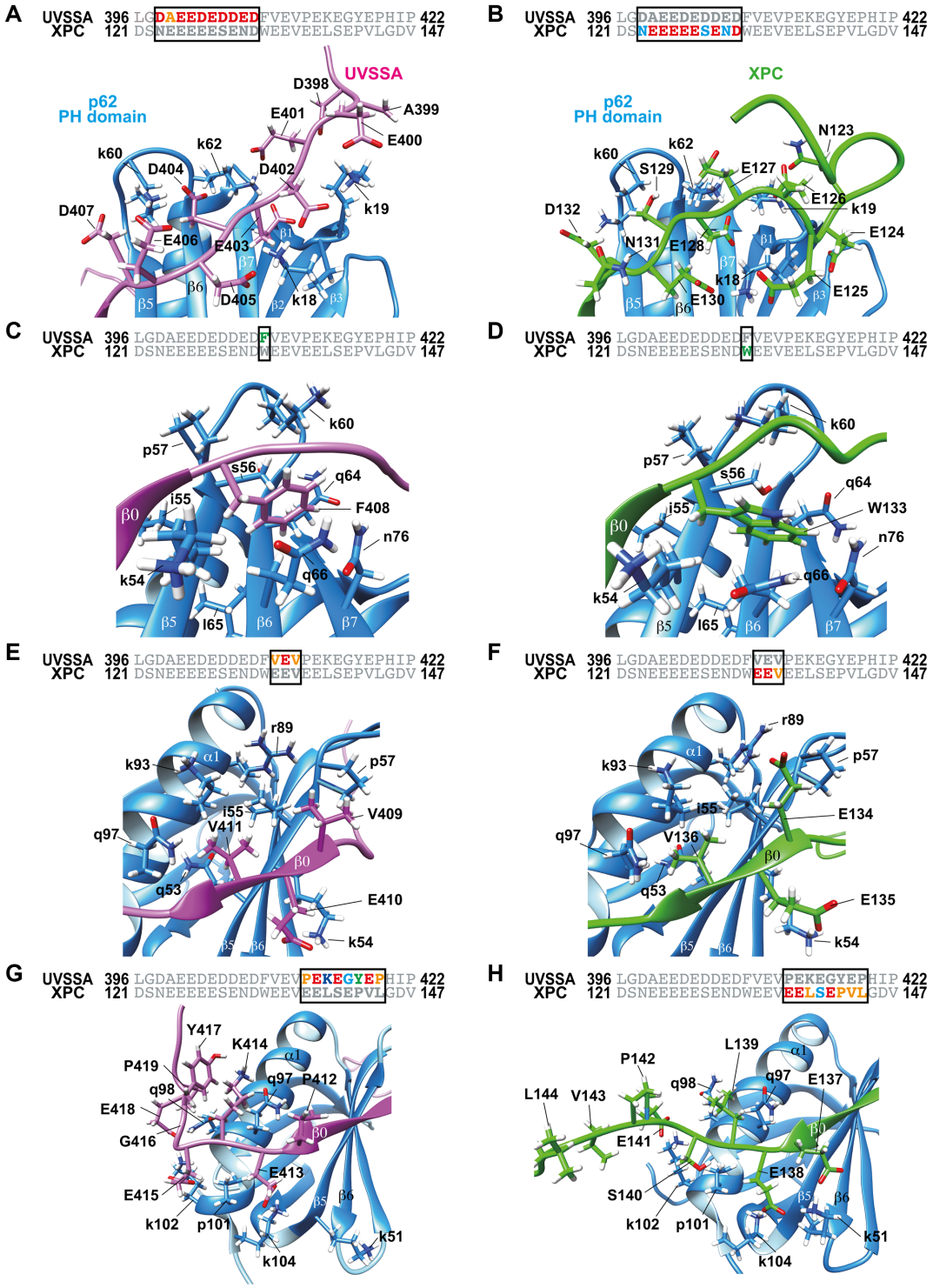

Figure 5. Comparison of p62 PH recognition between TCR factor UVSSA and GGR factor XPC. (**A**, **C**, **E**, **G**) Intermolecular interactions in the UVSSA–p62 PH complex. (**B**, **D**, **F**, **H**) Intermolecular interactions in the XPC–p62 PH complex. p62, UVSSA, and XPC are shown in blue, magenta, and green, respectively. To discriminate p62 from UVSSA or XPC, residues of p62 are labeled in lowercase and residues of UVSSA or XPC are labeled in uppercase.

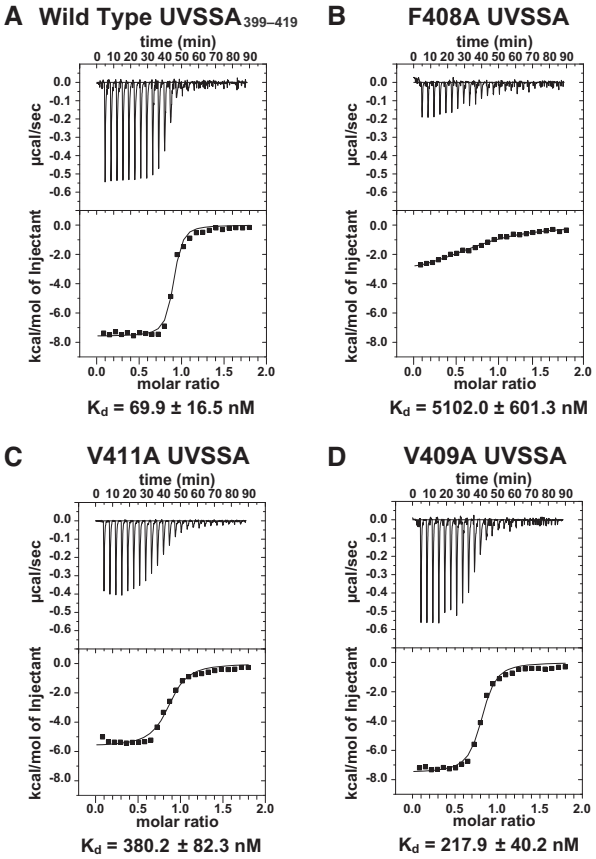

Figure 6. ITC analysis of p62 PH binding by UVSSA mutant. Shown are thermograms (upper panels) and binding isotherms (lower panels) of the calorimetric titration. (**A**) Titrant: wild type $UVSSA_{399–419}$. (**B**) Titrant: F408A $UVSSA_{399–419}$. (**C**) Titrant: V411A $UVSSA_{399–419}$. (**D**) Titrant: V409A $UVSSA_{399–419}$. The calculated binding dissociation constant (K_d) is shown below each panel. Data are the mean ± standard error (S.D.) from the fitting curve.

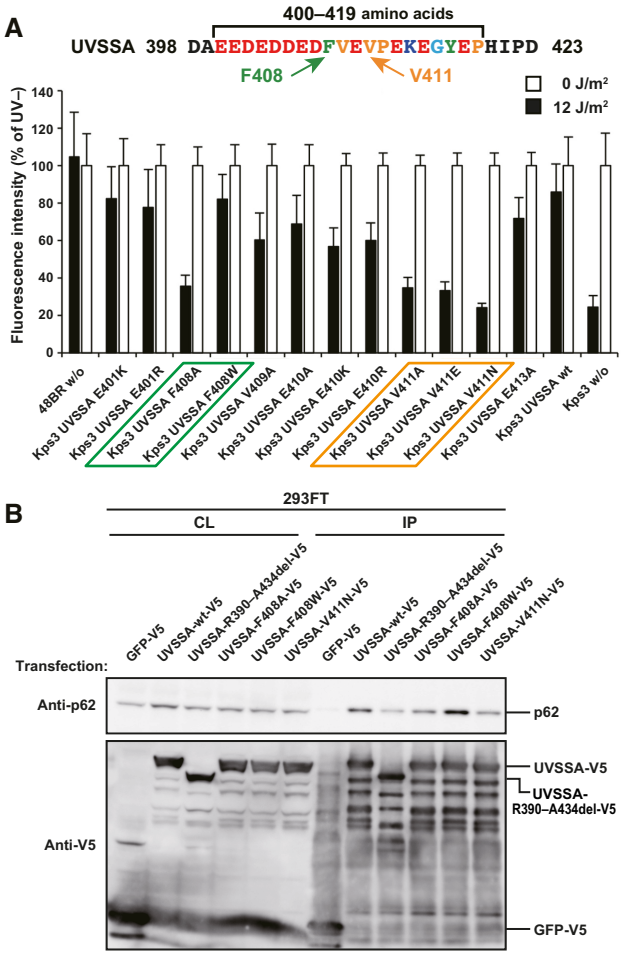

Figure 7. The p62 binding domain of UVSSA is essential for transcription coupled NER activity. (**A**) Recovery of RNA synthesis was measured in Kps3 cells expressing wild-type UVSSA–V5 or UVSSA–V5 with mutations in the p62-binding domain (filled bars, 12 J/m^2 of UV-C; open bars, no UV). Aromatic (green) and hydrophobic (orange) residues required for strong binding between UVSSA and p62 are indicated. Error bars represent the standard error (S.E.) of quadrupled experiments. (**B**) The interaction of p62 with either wild-type UVSSA or various UVSSA mutant proteins was assayed by immunoprecipitation, followed by western blotting. CL, crude lysate; IP, immunoprecipitate.

ordered acidic string. The acidic strings are polymorphic at the amino acid sequence level (Figure 1A), and hold no regular secondary structures in common; nevertheless, their networks of interaction with p62 PH highly resemble one another. Therefore, on the basis of three-dimensional structural information, rather than solely sequence information, we considered that it might be possible to identify a new p62 PH-binding partner.

Indeed, the presence of a sequence in the TCR initiation factor UVSSA with the potential to satisfy the common structural principles of p62 PH recognition led to the finding that UVSSA is responsible for recruiting TFIIH in TCR. The sequence, which is present at residues 400–413 in human UVSSA, is well conserved across different species (Figure 1A). Our finding is also consistent with a previous study showing that the deletion of residues 400–500 abolishes the interaction between UVSSA and TFIIH (22) (Figure 1B). In fact, this short sequence of UVSSA specifically binds to p62 PH with an affinity equivalent to XPC (Figure 2).

We carried out the ITC and NMR binding assays in buffer comprising 20 mM potassium phosphate (pH 6.8) in order to compare the binding of UVSSA with that of XPC under the same buffer conditions used in previous studies (26,50). Because this low salt concentration might not reflect binding under physiological conditions with higher salt concentration, we also performed the ITC assay in phosphate-buffered saline (PBS; 8.10 mM Na_2HPO_4, 1.47 mM KH_2PO_4, 137 mM NaCl, 2.68 mM KCl, pH 7.5). Although the binding affinity decreased as expected, the specific interaction of UVSSA with p62 PH was still retained (Supplementary Figure S3).

The strong interaction prompted us to determine the solution structure of the UVSSA–p62 PH complex (Figure 3), which revealed striking similarity to the XPC–p62 PH complex (Figures 4 and 5). Of note, substitution of a single amino acid of UVSSA caused a marked reduction in TCR activity, which correlated well with the strength of binding between the mutant and TFIIH p62 PH (Figures 6 and 7).

Such a correlation has been previously observed for XPC, where alanine substitution at a key residue for binding compromised UV resistance, recruitment of TFIIH to DNA damage sites, and removal of UV-induced photoproducts from genomic DNA (26). Both UVSSA and XPC interact with subunits of TFIIH other than p62, but the present results indicate that the interaction with p62 PH makes essential contributions to the recruitment of TFIIH in TCR and in GGR. Taking all of these findings together, we conclude that UVSSA is a TFIIH recruiting factor in TCR.

Our finding that UVSSA shares the binding surface of p62 PH in TFIIH with the GGR initiation factor XPC, and also with the transcription initiation factor TFIIE, provides a conceptual advance in our understanding of NER. In other words, because of the different mechanisms for recognition of DNA lesions in TCR and GGR, it might be imagined that different proteins would recruit TFIIH to damaged sites. However, their TFIIH recruiting mechanisms are remarkably similar. Because TFIIH is a huge complex comprising 10 different proteins, it may seem curious that UVSSA and XPC select such a small area on its large molecular surface. One possible explanation might come from the subsequent step in the NER process. In both TCR and GGR, recruitment of TFIIH is followed by loading of the incision nucleases XPG and XPF/ERCC1. It has been demonstrated that Rad4 (yeast homolog of XPC) competes with Rad2 (yeast homolog of XPG) for common binding sites on TFIIH, including the PH domain of Tfb1 (yeast homolog of p62) (25,53). XPG stabilizes TFIIH (54); however, the TFIIH–UVSSA complex does not contain XPG, implying that UVSSA and XPG share the same binding interface of TFIIH (15). We infer that UVSSA and XPC both use the same surface of TFIIH because it is efficient for passing TFIIH to XPG as it allows UVSSA or XPC to release from TFIIH at the same time that XPG associates with TFIIH. Further studies will be needed to verify this idea.

UVSSA has turned out to be a scaffold protein. Its N-terminal VHS domain supports a direct interaction with TFIIH and CSB after UV irradiation (15). The VHS domain is also required for its interaction with USP7 and CSA, regardless of UV damage (22). Furthermore, residues 151–495 together with a TRAF-binding motif (residues 251–254) are necessary for UVSSA's interaction with the TRAF domain of USP7 (23). In the present study, we have pinpointed a novel interaction between residues 399–419 and TFIIH p62 PH, and have reported the first structure of this complex. In parallel with finding new interactions of components of the TCR pathway, the identified interactions should be further characterized to define the details of their roles in TCR from both structural and functional points of view.

AVAILABILITY

Coordinates for the TFIIH p62–UVSSA complex have been deposited in the RCSB Protein Data Bank (PDB) under ID code 5XV8 and chemical shifts have been deposited in the BioMagResBank (BMRB) under accession number 36101.

SUPPLEMENTARY DATA

Supplementary Data are available at NAR Online.

FUNDING

Grants-in-Aid for Scientific Research on an NMR platform [07022019 to Y.Ni.] from the Ministry of Education, Culture, Sports, Science and Technology (MEXT), Japan; Platform for Drug Discovery, Informatics, and Structural Life Science [16am0101033j0004 to Y.Ni.] from the Japan Agency for Medical Research and Development (AMED), Japan; KAKENHI Grants-in-Aid for Scientific Research (C) [16K07277]) from the Japan Society for the Promotion of Science (JSPS) (to M.O.); KAKENHI (B) [26291005] from JSPS and the Practical Research Project for Rare/Intractable Diseases from AMED (to Y.Na., C.G., T.O.); KAKENHI Grants-in-Aid for Young Scientists (A) [15H05333] from JSPS (to Y.Na.); Special Coordination Funds for Promoting Science and Technology from the Japan Science and Technology Agency (JST) (to Y.Na.); KAKENHI grants-in-Aid for International Research Fellows [14F04093] from JSPS (to C.G.). Funding for open access charge: Japan Agency for Medical Research and Development.

Conflict of interest statement. None declared.

REFERENCES

1. Lehmann,A.R. (2003) DNA repair-deficient diseases, xeroderma pigmentosum, Cockayne syndrome and trichothiodystrophy. *Biochimie*, **85**, 1101–1111.
2. Shuck,S.C., Short,E.A. and Turchi,J.J. (2008) Eukaryotic nucleotide excision repair: from understanding mechanisms to influencing biology. *Cell Res.*, **18**, 64–72.
3. Naegeli,H. and Sugasawa,K. (2011) The xeroderma pigmentosum pathway: decision tree analysis of DNA quality. *DNA Repair*, **10**, 673–683.
4. Fousteri,M. and Mullenders,L.H. (2008) Transcription-coupled nucleotide excision repair in mammalian cells: molecular mechanisms and biological effects. *Cell Res.*, **18**, 73–84.
5. Hanawalt,P.C. and Spivak,G. (2008) Transcription-coupled DNA repair: two decades of progress and surprises. *Nat. Rev. Mol. Cell Biol.*, **9**, 958–970.
6. Sugasawa,K., Ng,J.M., Masutani,C., Iwai,S., van der Spek,P.J., Eker,A.P., Hanaoka,F., Bootsma,D. and Hoeijmakers,J.H. (1998) Xeroderma pigmentosum group C protein complex is the initiator of global genome nucleotide excision repair. *Mol. Cell*, **2**, 223–232.
7. Volker,M., Moné,M.J., Karmakar,P., van Hoffen,A., Schul,W., Vermeulen,W., Hoeijmakers,J.H., van Driel,R., van Zeeland,A.A. and Mullenders,L.H. (2001) Sequential assembly of the nucleotide excision repair factors in vivo. *Mol. Cell*, **8**, 213–224.
8. Keeney,S., Chang,G.J. and Linn,S. (1993) Characterization of a human DNA damage binding protein implicated in xeroderma pigmentosum E. *J. Biol. Chem.*, **268**, 21293–21300.
9. Takao,M., Abramic,M., Moos,M. Jr, Otrin,V.R., Wootton,J.C., McLenigan,M., Levine,A.S. and Protic,M. (1993) A 127 kDa component of a UV-damaged DNA-binding complex, which is defective in some xeroderma pigmentosum group E patients, is homologous to a slime mold protein. *Nucleic Acids Res.*, **21**, 4111–4118.
10. Yokoi,M., Masutani,C., Maekawa,T., Sugasawa,K., Ohkuma,Y. and Hanaoka,F. (2000) The xeroderma pigmentosum group C protein complex XPC-HR23B plays an important role in the recruitment of transcription factor IIH to damaged DNA. *J. Biol. Chem.*, **275**, 9870–9875.
11. Bernardes de Jesus,B.M., Bjørås,M., Coin,F. and Egly,J.M. (2008) Dissection of the molecular defects caused by pathogenic mutations in the DNA repair factor XPC. *Mol. Cell. Biol.*, **28**, 7225–7235.

12. Mathieu,N., Kaczmarek,N. and Naegeli,H. (2010) Strand- and site-specific DNA lesion demarcation by the xeroderma pigmentosum group D helicase. *Proc. Natl. Acad. Sci. U.S.A.*, **107**, 17545–17550.
13. Mellon,I., Spivak,G. and Hanawalt,P.C. (1987) Selective removal of transcription-blocking DNA damage from the transcribed strand of the mammalian DHFR gene. *Cell*, **51**, 241–249.
14. Sarasin,A. (2012) UVSSA and USP7: new players regulating transcription-coupled nucleotide excision repair in human cells. *Genome Med.*, **4**, 44.
15. Nakazawa,Y., Sasaki,K., Mitsutake,N., Matsuse,M., Shimada,M., Nardo,T., Takahashi,Y., Ohyama,K., Ito,K., Mishima,H. *et al.* (2012) Mutations in UVSSA cause UV-sensitive syndrome and impair RNA polymerase IIo processing in transcription-coupled nucleotide-excision repair. *Nat. Genet.*, **44**, 586–592.
16. Schwertman,P., Lagarou,A., Dekkers,D.H., Raams,A., van der Hoek,A.C., Laffeber,C., Hoeijmakers,J.H., Demmers,J.A., Fousteri,M., Vermeulen,W. *et al.* (2012) UV-sensitive syndrome protein UVSSA recruits USP7 to regulate transcription-coupled repair. *Nat. Genet.*, **44**, 598–602.
17. Zhang,X., Horibata,K., Saijo,M., Ishigami,C., Ukai,A., Kanno,S., Tahara,H., Neilan,E.G., Honma,M., Nohmi,T. *et al.* (2012) Mutations in UVSSA cause UV-sensitive syndrome and destabilize ERCC6 in transcription-coupled DNA repair. *Nat. Genet.*, **44**, 593–597.
18. Fujiwara,Y., Ichihashi,M., Kano,Y., Goto,K. and Shimizu,K. (1981) A new human photosensitive subject with a defect in the recovery of DNA synthesis after ultraviolet-light irradiation. *J. Invest. Dermatol.*, **77**, 256–263.
19. Itoh,T., Ono,T. and Yamaizumi,M. (1994) A new UV-sensitive syndrome not belonging to any complementation groups of xeroderma pigmentosum or Cockayne syndrome: siblings showing biochemical characteristics of Cockayne syndrome without typical clinical manifestations. *Mutat. Res.*, **314**, 233–248.
20. Itoh,T., Fujiwara,Y., Ono,T. and Yamaizumi,M. (1995) UVs syndrome, a new general category of photosensitive disorder with defective DNA repair, is distinct from xeroderma pigmentosum variant and rodent complementation group I. *Am. J. Hum. Genet.*, **56**, 1267–1276.
21. Spivak,G. (2005) UV-sensitive syndrome. *Mutat. Res.*, **577**, 162–169.
22. Fei,J. and Chen,J. (2012) KIAA1530 protein is recruited by Cockayne syndrome complementation group protein A (CSA) to participate in transcription-coupled repair (TCR). *J. Biol. Chem.*, **287**, 35118–35126.
23. Higa,M., Zhang,X., Tanaka,K. and Saijo,M. (2016) Stabilization of ultraviolet (UV)-stimulated scaffold protein A by interaction with ubiquitin-specific peptidase 7 is essential for transcription-coupled nucleotide excision repair. *J. Biol. Chem.*, **291**, 13771–13779.
24. Egly,J.M. and Coin,F. (2011) A history of TFIIH: two decades of molecular biology on a pivotal transcription/repair factor. *DNA Repair*, **10**, 714–721.
25. Lafrance-Vanasse,J., Arseneault,G., Cappadocia,L., Legault,P. and Omichinski,J.G. (2013) Structural and functional evidence that Rad4 competes with Rad2 for binding to the Tfb1 subunit of TFIIH in NER. *Nucleic Acids Res.*, **41**, 2736–2745.
26. Okuda,M., Kinoshita,M., Kakumu,E., Sugasawa,K. and Nishimura,Y. (2015) Structural insight into the mechanism of TFIIH recognition by the acidic string of the nucleotide excision repair factor XPC. *Structure*, **23**, 1827–1837.
27. Di Lello,P., Miller Jenkins,L.M., Mas,C., Langlois,C., Malitskaya,E., Fradet-Turcotte,A., Archambault,J., Legault,P. and Omichinski,J.G. (2008) p53 and TFIIEalpha share a common binding site on the Tfb1/p62 subunit of TFIIH. *Proc. Natl. Acad. Sci. U.S.A.*, **105**, 106–111.
28. Okuda,M., Tanaka,A., Satoh,M., Mizuta,S., Takazawa,M., Ohkuma,Y. and Nishimura,Y. (2008) Structural insight into the TFIIE-TFIIH interaction: TFIIE and p53 share the binding region on TFIIH. *EMBO J.*, **27**, 1161–1171.
29. Di Lello,P., Jenkins,L.M., Jones,T.N., Nguyen,B.D., Hara,T., Yamaguchi,H., Dikeakos,J.D., Appella,E., Legault,P. and Omichinski,J.G. (2006) Structure of the Tfb1/p53 complex: Insights into the interaction between the p62/Tfb1 subunit of TFIIH and the activation domain of p53. *Mol. Cell*, **22**, 731–740.
30. Okuda,M. and Nishimura,Y. (2014) Extended string binding mode of the phosphorylated transactivation domain of tumor suppressor p53. *J. Am. Chem. Soc.*, **136**, 14143–14152.
31. Mas,C., Lussier-Price,M., Soni,S., Morse,T., Arseneault,G., Di Lello,P., Lafrance-Vanasse,J., Bieker,J.J. and Omichinski,J.G. (2011) Structural and functional characterization of an atypical activation domain in erythroid Kruppel-like factor (EKLF). *Proc. Natl. Acad. Sci. U.S.A.*, **108**, 10484–10489.
32. Okuda,M., Araki,K., Ohtani,K. and Nishimura,Y. (2016) The interaction mode of the acidic region of the cell cycle transcription factor DP1 with TFIIH. *J. Mol. Biol.*, **428**, 4993–5006.
33. Lecoq,L., Raiola,L., Chabot,P.R., Cyr,N., Arseneault,G., Legault,P. and Omichinski,J.G. (2017) Structural characterization of interactions between transactivation domain 1 of the p65 subunit of NF-κB and transcription regulatory factors. *Nucleic Acids Res.*, **45**, 5564–5576.
34. Di Lello,P., Nguyen,B.D., Jones,T.N., Potempa,K., Kobor,M.S., Legault,P. and Omichinski,J.G. (2005) NMR structure of the amino-terminal domain from the Tfb1 subunit of TFIIH and characterization of its phosphoinositide and VP16 binding sites. *Biochemistry*, **44**, 7678–7686.
35. Langlois,C., Mas,C., Di Lello,P., Jenkins,L.M., Legault,P. and Omichinski,J.G. (2008) NMR structure of the complex between the Tfb1 subunit of TFIIH and the activation domain of VP16: structural similarities between VP16 and p53. *J. Am. Chem. Soc.*, **130**, 10596–10604.
36. Chabot,P.R., Raiola,L., Lussier-Price,M., Morse,T., Arseneault,G., Archambault,J. and Omichinski,J.G. (2014) Structural and functional characterization of a complex between the acidic transactivation domain of EBNA2 and the Tfb1/p62 Subunit of TFIIH. *PLoS Pathog.*, **10**, e1004042.
37. Delaglio,F., Grzesiek,S., Vuister,G.W., Zhu,G., Pfeifer,J. and Bax,A. (1995) NMRPipe: A multidimensional spectral processing system based on UNIX pipes. *J. Biomol. NMR*, **6**, 277–293.
38. Johnson,B.A. and Blevins,R.A. (1994) NMRView: a computer program for the visualization and analysis of NMR data. *J. Biomol. NMR*, **4**, 603–614.
39. Cavanagh,J., Fairbroher,W.J., Palmer,III A.G. and Skelton,N.J. (1996) *Protein NMR Spectroscopy*. Academic Press, San Diego.
40. Cornilescu,G., Delaglio,F. and Bax,A. (1999) Protein backbone angle restraints from searching a database for chemical shift and sequence homology. *J. Biomol. NMR*, **13**, 289–302.
41. Brünger,A.T. (1993) *X-PLOR Version 3.1: A System for X-ray crystallography and NMR*. Yale University Press, New Haven.
42. Schwieters,C.D., Kuszewski,J.J., Tjandra,N. and Clore,G.M. (2003) The Xplor-NIH NMR molecular structure determination package. *J. Magn. Reson.*, **160**, 65–73.
43. Linge,J.P., Williams,M.A., Spronk,C.A., Bonvin,A.M. and Nilges,M. (2003) Refinement of protein structures in explicit solvent. *Proteins*, **50**, 496–506.
44. Laskowski,R.A., Rullmann,J.A.C., MacArthur,M.W., Kaptein,R. and Thornton,J.M. (1996) AQUA and PROCHECK-NMR: programs for checking the quality of protein structures solved by NMR. *J. Biomol. NMR*, **8**, 477–486.
45. Pettersen,E.F., Goddard,T.D., Huang,C.C., Couch,G.S., Greenblatt,D.M., Meng,E.C. and Ferrin,T.E. (2004) UCSF Chimera–a visualization system for exploratory research and analysis. *J. Comput. Chem.*, **25**, 1605–1612.
46. Meng,E.C., Pettersen,E.F., Couch,G.S., Huang,C.C. and Ferrin,T.E. (2006) Tools for integrated sequence-structure analysis with UCSF Chimera. *BMC Bioinformatics*, **7**, 339.
47. Nakazawa,Y., Yamashita,S., Lehmann,A.R. and Ogi,T. (2010) A semi-automated non-radioactive system for measuring recovery of RNA synthesis and unscheduled DNA synthesis using ethynyluracil derivatives. *DNA Repair*, **9**, 506–516.
48. Jia,N., Nakazawa,Y., Guo,C., Shimada,M., Sethi,M., Takahashi,Y., Ueda,H., Nagayama,Y. and Ogi,T. (2015) A rapid, comprehensive system for assaying DNA repair activity and cytotoxic effects of DNA-damaging reagents. *Nat. Protoc.*, **10**, 12–24.
49. Okuda,M., Higo,J., Komatsu,T., Konuma,T., Sugase,K. and Nishimura,Y. (2016) Dynamics of the extended string-like interaction of TFIIE with the p62 subunit of TFIIH. *Biophys. J.*, **111**, 950–962.
50. Okuda,M. and Nishimura,Y. (2015) Real-time and simultaneous monitoring of the phosphorylation and enhanced interaction of p53

and XPC acidic domains with the TFIIH p62 subunit. *Oncogenesis*, **4**, e150.
51. Gervais,V., Lamour,V., Jawhari,A., Frindel,F., Wasielewski,E., Dubaele,S., Egly,J.M., Thierry,J.C., Kieffer,B. and Poterszman,A. (2004) TFIIH contains a PH domain involved in DNA nucleotide excision repair. *Nat. Struct. Mol. Biol.*, **11**, 616–622.
52. Burley,S.K. and Petsko,G.A. (1986) Amino-aromatic interactions in proteins. *FEBS Lett.*, **203**, 139–143.
53. Lafrance-Vanasse,J., Arseneault,G., Cappadocia,L., Chen,H.T., Legault,P. and Omichinski,J.G. (2012) Structural and functional characterization of interactions involving the Tfb1 subunit of TFIIH and the NER factor Rad2. *Nucleic Acids Res.*, **40**, 5739–5750.
54. Ito,S., Kuraoka,I., Chymkowitch,P., Compe,E., Takedachi,A., Ishigami,C., Coin,F., Egly,J.M. and Tanaka,K. (2007) XPG stabilizes TFIIH, allowing transactivation of nuclear receptors: implications for Cockayne syndrome in XP-G/CS patients. *Mol. Cell*, **26**, 231–243.
55. Fukuchi,S., Sakamoto,S., Nobe,Y., Murakami,S.D., Amemiya,T., Hosoda,K., Koike,R., Hiroaki,H. and Ota,M. (2012) IDEAL: Intrinsically Disordered proteins with Extensive Annotations and Literature. *Nucleic Acids Res.*, **40**, D507–D511.